Published in final edited form as:
Mach Learn Med Imaging. 2014 ; 8679: 198–206. doi:10.1007/978-3-319-10581-9_25.

Deformation field correction for spatial normalization of PET images using a population-derived partial least squares model

Murat Bilgel[1,2], **Aaron Carass**[1], **Susan M. Resnick**[2], **Dean F. Wong**[3], and **Jerry L. Prince**[1,3]

[1]Image Analysis and Communications Lab., Johns Hopkins University

[2]Lab. of Behavioral Neuroscience, National Institute on Aging, NIH

[3]Dept. of Radiology, Johns Hopkins University School of Medicine, Baltimore, MD, USA

Abstract

Spatial normalization of positron emission tomography (PET) images is essential for population studies, yet work on anatomically accurate PET-to-PET registration is limited. We present a method for the spatial normalization of PET images that improves their anatomical alignment based on a deformation correction model learned from structural image registration. To generate the model, we first create a population-based PET template with a corresponding structural image template. We register each PET image onto the PET template using deformable registration that consists of an affine step followed by a diffeomorphic mapping. Constraining the affine step to be the same as that obtained from the PET registration, we find the diffeomorphic mapping that will align the structural image with the structural template. We train partial least squares (PLS) regression models within small neighborhoods to relate the PET intensities and deformation fields obtained from the diffeomorphic mapping to the structural image deformation fields. The trained model can then be used to obtain more accurate registration of PET images to the PET template without the use of a structural image. A cross validation based evaluation on 79 subjects shows that our method yields more accurate alignment of the PET images compared to deformable PET-to-PET registration as revealed by 1) a visual examination of the deformed images, 2) a smaller error in the deformation fields, and 3) a greater overlap of the deformed anatomical labels with ground truth segmentations.

Keywords

PET registration; deformation field; partial least squares

1 Introduction

Deformable medical image registration is essential to aligning a population of images, performing voxelwise association studies, and tracking longitudinal changes. While within-modality spatial normalization of structural medical images has been studied extensively, work on anatomically accurate positron emission tomography (PET) spatial normalization remains limited. The anatomical alignment of PET images is a difficult problem since they reflect metabolism and function rather than anatomy, the observed intensities depend on the amount of radiotracer used, and the spatial detail is confounded by radiotracer spillover.

Whenever available, it is preferable to use a structural image (such as a T_1-weighted MRI) co-registered with the subject's PET image for registration purposes and to warp the PET image accordingly. However, it is important to be able to perform PET spatial normalization accurately without guidance from additional images, as structural MR images are not always available due to claustrophobia or MR-incompatible implants. Enabling accurate PET spatial normalization can obviate the need for structural imaging in certain studies, resulting in lower costs, hospitalization time, and patient burden.

Prior work on PET spatial normalization includes modification of the target image intensities using a whole-brain principal component analysis model to match more closely to the moving image intensities [7, 9], imposing constraints on the PET deformations via a statistical control point model based on the deformation parameters of PET-to-MR registrations [8], and making use of the 4D data available in dynamic PET studies [3]. While these approaches show improvements over simple 3D PET spatial normalization, they do not take into account the systematic errors present in PET-to-PET registration due to the incorrect inference of anatomical boundaries stemming from spillover effects and the preferential binding of the radiotracer to certain parts within structures.

We present a method for the spatial normalization of PET images based on a deformationcorrection model learned from structural image registration. The observation motivating our method is: *PET-to-PET registration produces deformations that are systematically biased in certain regions, and these biases can be characterized as a function of location and estimated within small neighborhoods*. The correction operates on the PET-to-PET deformation fields obtained from a deformable registration algorithm and uses partial least squares regression models learned from a population of subjects relating the local PET intensities and deformation fields to the corresponding structural imaging deformation fields. The learned relationship between the deformation fields accounts for the anatomical inaccuracies present in the alignment of PET images, while the use of PET intensity information allows for inter-subject variability in radiotracer binding due to differences in physiology.

2 Method

To construct our model, we need the deformation fields that are to be applied to the PET images and their structural counterparts to bring the images to a common template. Our model is then trained using the resulting deformation fields for the PET and the structural images as well as the warped PET image intensities, yielding a correction that can be applied to PET deformation fields.

2.1 Image template generation

To create an anatomically accurate PET template image, we rely on the associated structural images. The structural images $S_i (i = 1, \ldots, N)$, are co-registered rigidly with the subject PET images F_i yielding transformation $\boldsymbol{R}_i$ followed by affine registration to a common space with transformation $\boldsymbol{T}_i$.

The affinely coregistered structural images $\hat{S}_i = S_i (\boldsymbol{R}_i \circ \boldsymbol{T}_i)$ are then used to create a structural population template image $\bar{S}$. Let $\boldsymbol{x}$ be in the common space Ω, and φ_i a diffeomorphism defined on Ω to transform $\hat{S}_i$ into a new coordinate system by $\hat{S}_i \circ \varphi_i(\boldsymbol{x}, t)$, with $t \in [0, 1]$ and $\varphi_i(\boldsymbol{x}, 0) = \boldsymbol{x}$. The square-integrable and continuous vector field $\boldsymbol{v}_i(\boldsymbol{x}, t)$ parameterizes the diffeomorphism such that $\frac{d\phi_i(\boldsymbol{x},t)}{dt} = \boldsymbol{\nu}_i(\phi_i(\boldsymbol{x},t),t)$ [1]. The population template is

$$\overline{S}, \{\phi_i\} = \underset{\overline{S},\{\phi_i\}}{\arg\min} \sum_{i=1}^{N} \left(\int_0^1 \| \boldsymbol{\nu}_i(\boldsymbol{x},t) \|_L^2 dt + \int_\Omega - \mathrm{CC}(\overline{S}, \hat{S}_i(\phi_i), \boldsymbol{x}) d\Omega \right) \quad (1)$$

where L is a Gaussian convolution operator regularizing the velocity field, and $\mathrm{CC}(\bar{S}, \hat{S}_i(\varphi_i), \boldsymbol{x})$ is the cross correlation similarity measure with the inner products calculated over a cubic window around $\boldsymbol{x}$ [2].

The affine transformations T_i and diffeomorphisms φ_i obtained from the structural image template construction are applied to the corresponding PET images in order to bring them into the same template space. The PET template $\bar{F}$ is then defined as the mean of the spatially normalized PET images as

$$\overline{F} = \frac{1}{N} \sum_{i=1}^{N} F_i(\boldsymbol{T}_i \circ \phi_i). \quad (2)$$

2.2 Computing a training set

Using a set of subjects for whom both a structural image and a PET image are available,we perform deformable registration to map the PET images onto the PET template. For each subject $i = 1, \ldots, n$ in the training data, the deformable registration consists of an affine transformation $\boldsymbol{T}_i'$ followed by a diffeomorphic mapping $\boldsymbol{\psi}_i(\boldsymbol{x})$ defined on Ω. We denote the PET image registered onto the PET template $\bar{F}$ by $\tilde{F}_i = F_i(\boldsymbol{T}_i' \circ \boldsymbol{\psi}_i)$. Constraining the affine transformation to be the same as that obtained from the PET-to-PET registration, we then perform another registration to find the deformation field $\boldsymbol{\phi}_i(\boldsymbol{x})$ that must be applied to the structural image such that $S_i(\boldsymbol{R}_i \circ \boldsymbol{T}_i' \circ \boldsymbol{\varphi}_i)$ is in alignment with the structural image template $\bar{S}$.

2.3 Model training

Our goal is to train a model at each voxel $\boldsymbol{x} \in \Omega$ describing a relationship between the estimated PET deformation field $\boldsymbol{\psi}_i(\boldsymbol{x})$ and the structural image deformation field $\boldsymbol{\phi}_i(\boldsymbol{x})$ for the training subjects $i = 1,\ldots, n$. To account for the variability in PET intensities across subjects due to differences in function and metabolism, we also include the intensities $\tilde{F}_i(\boldsymbol{x})$ as features in the model.

We denote the row vector whose components are the warped PET intensities at each voxel in the neighborhood $\mathcal{N}(\boldsymbol{x})$ as $\tilde{F}_i \mathcal{N}(\boldsymbol{x})) \in \mathbb{R}^{\| \mathcal{N}\|}$, where $\| \mathcal{N}\|$ is the number of voxels in the

neighborhood. Similarly, we denote the row vector whose components are the deformation field components at each voxel in the neighborhood as $\psi_i(\mathcal{N}(\boldsymbol{x})) \in \mathbb{R}^{3\|\mathcal{N}\|}$. In our setup, we use the input features $\mathbf{X}(\boldsymbol{x}) \in \mathbb{R}^{n \times 4\|\mathcal{N}\|}$ and the output data $\mathbf{Y}(\boldsymbol{x}) \in \mathbb{R}^{n \times 3}$

$$\mathbf{X}(\boldsymbol{x}) = \begin{bmatrix} \vdots & \vdots \\ \psi_i(\mathcal{N}(\boldsymbol{x})) & \tilde{F}_i(\mathcal{N}(\boldsymbol{x})) \\ \vdots & \vdots \end{bmatrix} \quad \mathbf{Y}(\boldsymbol{x}) = \begin{bmatrix} \vdots \\ \varphi_i(\boldsymbol{x}) \\ \vdots \end{bmatrix} \quad (3)$$

compiled across the *n* subjects to train a partial least squares regression model for predicting the structural image deformation vector at the center voxel.

Partial least squares (PLS) is a dimensionality reduction technique that seeks to find asmall number of latent variables extracted from the input features that best explain the observed data [10]. The number of *latent variables*, or *components*, to be retained in the model is denoted by c. PLS performs linear decomposition of the input features $\mathbf{X} \in \mathbb{R}^{n \times p}$ and observed data $\mathbf{Y} \in \mathbb{R}^{n \times q}$, where *n*, *p*, and *q* are the number of observations, input features, and output features, respectively, to obtain $\mathbf{X} = \mathbf{T}\mathbf{P}^T + \mathbf{V}$ and $\mathbf{Y} = \mathbf{U}\mathbf{Q}^T + \mathbf{W}$, where **T** and **U** are the $n \times c$ *score matrices* each consisting of orthogonal columns, with *loadings* **P** and **Q**, and *residuals* **V** and **W**. PLS finds the linear decompositions so that the covariance of the extracted score matrices is maximized. The coefficient matrix for the multivariate linear regression of **X** on **Y** is then given by $\mathbf{B} = \mathbf{X}^T\mathbf{U}\,(\mathbf{T}^T\,\mathbf{X}\mathbf{X}^T\mathbf{U})^{-1}\,\mathbf{T}^T\mathbf{Y}$ [10], which is later used for prediction.

The choice of the number of components *c* is important: a small value will yield a model that cannot account for the sample variance while a large value will lead to over-fitting. We apply a *k*-fold cross validation as part of the training to determine the best number of PLS components to retain in our model. The cross validation involves splitting the training subjects into *k* groups, one of which is used to test the model that is trained on the remaining $k - 1$. This training and testing procedure is repeated to obtain predictions on each of the *k* groups. We find an optimal $\hat{c}$ for each spatial location using the cross validation results:

$$\hat{c}(\boldsymbol{x}) = \arg\min_{c} \sum_{i=1}^{n} \| \hat{\varphi}_i(\boldsymbol{x}; c) - \varphi_i(\boldsymbol{x}) \|^2. \quad (4)$$

Here, $\hat{\varphi}_i(\boldsymbol{x}; c)$ is the prediction of the PLS model with c components for test subject *i*. We use this spatially varying choice $\hat{c}(\boldsymbol{x})$ in the model at each voxel $\boldsymbol{x}$.

3 Results

PET scans were performed on a GE Advance scanner immediately following an intravenous bolus injection of Pittsburgh compound B (PiB), which binds to the beta-amyloid peptide. Dynamic PET data were acquired over 70 minutes, yielding 33 time frames each with 128 × 128 × 35 voxels. Voxel size was 2 × 2 × 4.25 mm^3. Each time frame was cropped to 118 × 118 × 33 images. The images corresponding to the first 20 minutes were averaged to create a static PET image for each subject. Early time frames were chosen as they are mostly

reflective of cerebral blood flow and show clearer anatomic boundary less vulnerable to modification by beta-amyloid. For structural images, we used MPRAGE scans performed on a Philips Achieva 3T scanner with the following acquisition parameters: TR = 6.8 ms, TE = 3.2 ms, $\alpha = 8°$ flip angle, 256 × 256 matrix, 170 sagittal slices, 1 × 1 mm^2 in-plane pixel size, 1.2 mm slice thickness. Three subjects had their MPRAGE scan 4 years after the PET, and one subject 2 years after the PET. The remaining subjects had both scans during the same visit.

The inhomogeneity corrected [11] MPRAGE images for each subject were rigidly aligned onto the corresponding static PET and skull-stripped [4]. The intensities of the PET images were normalized by the mean intensity within the volume, and thresholded at 80% to remove background noise. The MPRAGE and PET population templates were constructed using the ANTs package using 79 subjects (http://picsl.upenn.edu/software/ants/). The diffeomorphic registration of each subject onto the population template was performed using SyN [1], with the same parameters for MPRAGE and PET. The model was validated using 10-fold cross validation on 79 subjects. Input features for PLS were obtained over 3 × 3 × 3 neighborhoods, and within each training set, an additional k = 10-fold cross validation was used to pick the number of components to keep in the model.

We compared our method against PET-to-PET template registration and an implementation of [7] that involved first creating a PET template using corresponding MRIs as in our approach, constructing a whole-brain PCA model from the spatially normalized PET images, affinely registering the subject's PET onto the template, modifying the template using the PCA model to resemble more closely to the subject, and finally performing deformable registration using the modified template. Sample PET and MPRAGE images warped by deformation fields obtained from the different methods are presented in Fig. 1. Ventricle size is overestimated in both PET-to-PET registration and the method described in [7], whereas our method achieves better registration as revealed by the difference images. The putamen, a structure that exhibits higher activity in the PET image and thus causes spillover, is also better aligned by our method.

A comparison of the root mean square (RMS) error of the deformation fields is presented in Fig. 2. The deformation field ϕ obtained from the registration of MPRAGE onto the MPRAGE template is used as ground truth in the RMS error calculation. Our method achieves the lowest overall RMS error.

To assess the accuracy of anatomical alignment, the FreeSurfer [5] segmentations of the original MPRAGE images were brought into the template space by applying the mappings from the previously performed registrations. Using the FreeSurfer labels deformed according to ϕ as ground truth, we calculated the Dice coefficients [6] for the deformed labels. Table 1 shows the summary statistics for Dice coefficients for gray matter, white matter, and ventricular corticospinal fluid (CSF). Dice coefficients for our method are statistically different ($p < 0.01$ for all three tissue types) from both compared methods. Fig. 3 shows the Dice coefficient box plots for cortical regions. While the method proposed by [7] yields mixed results, our method consistently achieves higher Dice coefficients than either of the methods compared against. Dice coefficients for our method are statistically different

($p < 0.05$) from both compared methods for all regions except for cuneus, paracentral lobule, precentral gyrus and temporal pole.

4 Discussion and Conclusion

In our dataset, PET-to-PET registration consistently yielded larger ventricles compared to MPRAGE-to-MPRAGE registration. We also observed smaller brains and larger subcortical gray structures in PET-to-PET registered volumes, but these effects were subtle (Fig. 1).

We presented a deformation correction method to improve the anatomical alignment of PET images. Cross validation results show that our deformation correction method reduces the deformation field error and improves the anatomical alignment of PET images as evidenced by the higher Dice coefficients calculated using the deformed segmentations. Our method can compensate for errors in PET-to-PET registration by learning locally from the structural image registrations. While we used SyN for registration purposes, the method can be applied to any deformable PET-to-PET registration method.

Our method is particularly suited for spatial normalization of PET images in datasets where only a subset of the subjects have structural images. Subjects with both PET and structural images can be used to train the model, and those with PET images only can then be registered onto the PET template, taking into account the deformation correction provided by the model. If the dataset contains no concurrent PET and structural images, our deformation correction can still be applied given a PET template and an associated deformation field correction model that has already been constructed using a separate dataset.

The proposed approach could be applied to improve the deformable registration of other types of medical images with low resolution, poor contrast, geometric distortions, or inadequate anatomical content by using a model trained on corresponding medical images that are largely free of such effects.

Acknowledgments

This research was supported in part by the Intramural Research Program of the NIH.

References

1. Avants BB, Epstein CL, Grossman M, Gee JC. Symmetric diffeomorphic image registration with cross-correlation: evaluating automated labeling of elderly and neurodegenerative brain. Medical Image Analysis. 2008; 12(1):26–41. [PubMed: 17659998]
2. Avants BB, Yushkevich P, Pluta J, Minkoff D, Korczykowski M, Detre J, Gee JC. The optimal template effect in hippocampus studies of diseased populations. Neurolmage. 2010; 49(3):2457–66.
3. Bieth, M.; Reader, AJ.; Siddiqi, K. Atlas construction for dynamic (4D) PET using diffeomorphic transformations. In: Mori, K.; Sakuma, I.; Sato, Y.; Barillot, C.; Navab, N., editors. MICCAI 2013, LNCS. Vol. 8150. Springer Berlin Heidelberg; 2013. p. 35-42.
4. Carass A, Cuzzocreo J, Wheeler MB, Bazin PL, Resnick SM, Prince JL. Simple paradigm for extra-cerebral tissue removal: algorithm and analysis. Neurolmage. 2011; 56(4):1982–92.
5. Desikan RS, Ségonne F, Fischl B, Quinn BT, Dickerson BC, Blacker D, Buckner RL, Dale AM, Maguire RP, Hyman BT, Albert MS, Killiany RJ. An automated labeling system for subdividing the

human cerebral cortex on MRI scans into gyral based regions of interest. Neurolmage. 2006; 31(3): 968–80.

6. Dice LR. Measures of the amount of ecologic association between species. Ecology. 1945; 26(3): 297–302.
7. Fripp J, Bourgeat P, Acosta O, Jones G, Villemagne V, Ourselin S, Rowe C, Salvado O. Generative atlases and atlas selection for C11-PIB PET-PET registration of elderly, mild cognitive impaired and Alzheimer disease patients. ISBI 2008. 2008:1155–1158.
8. Fripp, J.; Bourgeat, P.; Raniga, P.; Acosta, O.; Villemagne, V.; Jones, G.; O'Keefe, G.; Rowe, C.; Ourselin, S.; Salvado, O. MR-less high dimensional spatial normalization of 11C PiB PET images on a population of elderly, mild cognitive impaired and Alzheimer disease patients. In: Metaxas, D.; Axel, L.; Fichtinger, G.; Székely, G., editors. MICCAI 2008, LNCS. Vol. 5241. Springer Berlin Heidelberg; 2008. p. 442-449.
9. Lundqvist R, Lilja J, Thomas BA, Lötjönen J, Villemagne VL, Rowe CC, Thurfjell L. Implementation and validation of an adaptive template registration method for 18F-flutemetamol imaging data. Journal of Nuclear Medicine. 2013; 54(8):1472–1478. [PubMed: 23740104]
10. Rosipal, R.; Krämer, N. Overview and recent advances in partial least squares. In: Saunders, C.; Grobelnik, M.; Gunn, S.; Shawe-Taylor, J., editors. SLSFS, LNCS. Vol. 3940. Springer Berlin Heidelberg; 2006. p. 34-51.
11. Sled JG, Zijdenbos AP, Evans AC. A nonparametric method for automatic correction of intensity nonuniformity in MRI data. TMI. 1998; 17(1):87–97.

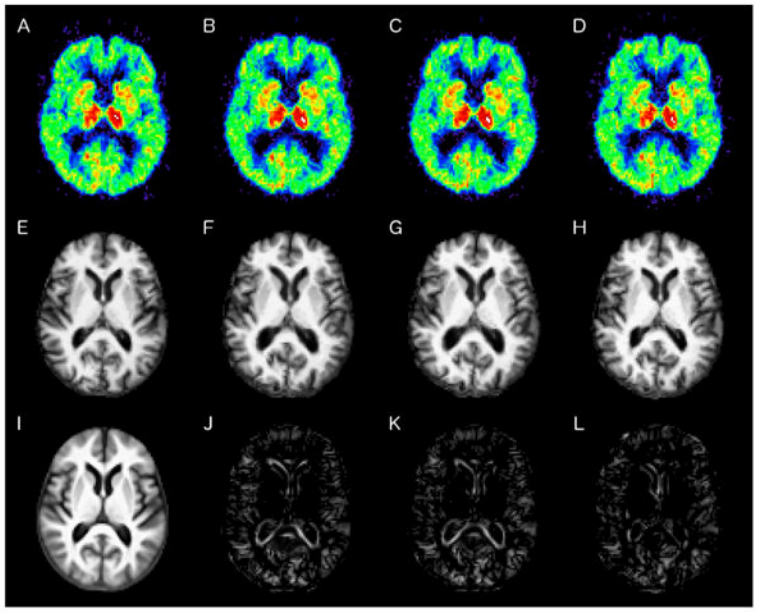

Fig.1.

Visual comparison of deformed images for a sample subject. First row: PET deformed using (A) the deformation ϕ from MPRAGE-to-MPRAGE template registration, (B) the deformation ψ from PET-to-PET template registration, (C) the deformation given by [7] (D) the deformation $\hat{\phi}$ predicted using our PLS model. Second row: MPRAGE deformed using (E) ϕ, (F) ψ, (G) the deformation given by [7] and (H) $\hat{\phi}$. Third row: (I) MPRAGE template, (J) difference of E and F, (K) difference of E and G (L) difference of E and H.

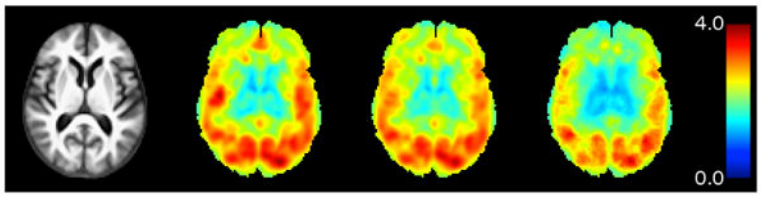

Fig.2.

Root mean square (RMS) error (in mm) of the PET deformation fields, calculated across 79 subjects. Left to right: MPRAGE template, RMS error of ψ, RMS error of the deformation given by [7], and RMS error of $\hat{\phi}$ predicted using our PLS model.

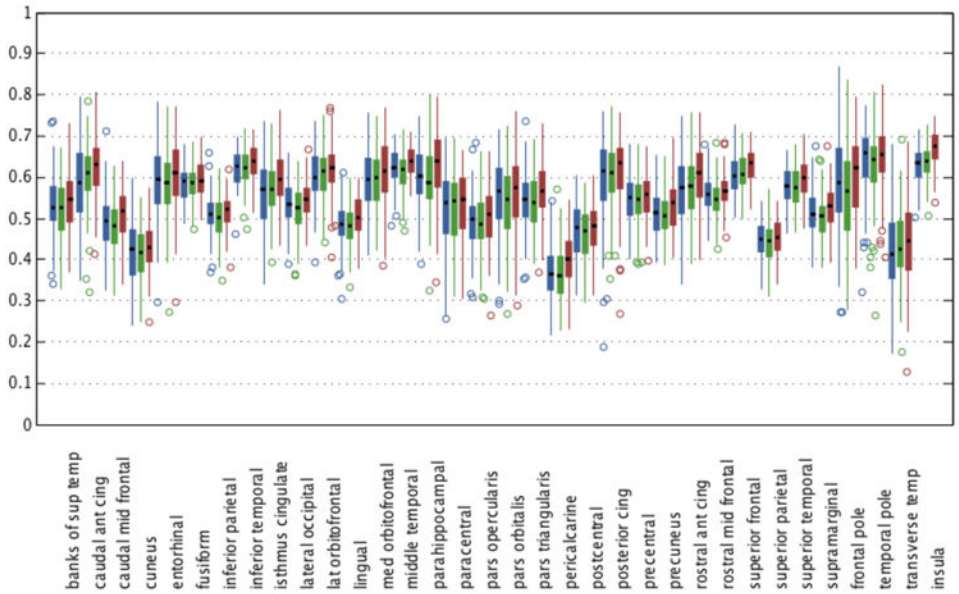

Fig.3.

Box plots of Dice coefficients for cortical labels across 79 subjects calculated using the deformations obtained from PET-to-PET registration (blue), the method proposed by [7] (green), and our method (red).

Table 1

Dice coefficients (mean ± st. dev., $N = 79$) for major brain tissue types.

	PET-to-PET	PCA method by [7]	Our method
Gray matter	0.64 ± 0.02	0.64 ± 0.03	0.65 ± 0.02
White matter	0.76 ± 0.02	0.76 ± 0.02	0.78 ± 0.02
Ventricular CSF	0.77 ± 0.05	0.78 ± 0.04	0.80 ± 0.04